ISSN 1392–1320 MATERIALS SCIENCE (MEDŽIAGOTYRA). Vol. 21, No. 2. 2015

Morphology Analysis of Cu Film Fractures in Sandwiched Methylmethacrylate Plates

Cristiano FIDANI [1] *, Maurizio De CRESCENZI [2]

[1] *Osservatorio Sismico "A. Bina", Borgo XX Giugno, 74, 06121, Perugia, Italy*
[2] *Dipartimento di Fisica, Università di Roma Tor Vergata, Via della Ricerca Scientifica 1, 00133, Roma, Italy*

crossref http://dx.doi.org/10.5755/j01.mm.21.2.6518

Received 22 February 2014; accepted 20 May 2014

Thin films of Cu were evaporated on solid plates of polymethylmethacrylate (PMMA). A successive polymerization process was made to realize sandwiched structure to protect the Cu films. Fracturing of the metal film surface was observed with several morphologies showing two different fracture systems. Surface film morphology was analysed in terms of the distribution area of the islands and contour fractal dimension. The island area showed a maximum corresponding to 42 nm of the Cu thickness, which was a threshold to observe two main fracture systems. The fractures pattern resulted to be scale invariant with fractal dimension between 1.55 and 1.7. The minimum fractal dimension also depended from the film thickness and corresponded to the maximum of the island areas. The reported effects can be understood on the basis of different thermal expansion coefficients of the two materials, their thermally induced adhesion and the action of the monomer.
Keywords: copper thin films, e-beam evaporation, deposition thickness, polymethylmethacrylate, surface analysis.

1. INTRODUCTION

Deposition of thin films of several metallic materials on polymer surfaces is frequently used to obtain mirrors with selective properties for reflectivity and transmission of visible light [1]. Nowadays the thin metal films are widely used for industrial products of many objects ranging from reflector for car lights, compact discs and electrically shielded computer cases to foils for food packing [2]. Finally, the deposition of thin metallic films on polymers are of primary importance both for active and passive use, to increase the chemical-physical properties of the objects [3]; while the sandwiched structure are built to increase bending stiffness and bending strength [4].

Generally, several metallic-based paints [5] give a wide range of colours and effects when mixed with the pre-polymer. When these paints are used as films, they are generally deposited after that the polymer, used as substrate, has been modelled to obtain the desired object. These methods intrinsically suffer of the non uniformity of coverage induced by the non regular shape of the object. For this reason, the use of sandwiched plates with metal cores, can constitute a valid solution to overcome the undesired effect of inhomogeneity.

Several methods of deposition are now available by epitaxial growth, namely: electro-deposition, electro-less deposition, sol-gel deposition, nano-particle growth and crystallization, chemical precipitation, chemical vapour deposition and vacuum thermal evaporation [6]. The possibilities offered by the vacuum technology are now well established and await for a wider use in the industrial processes [3, 7].

A fundamental problem to be solved still remains the protection of the metallic films from the oxidation and mechanical scratches. A valid solution can be found in the sandwiched structures that can be realized by a subsequent polymerization. However, this process modify strongly the morphology of the film surfaces depending from the chemical-physical condition of the polymerization and metallic thickness. The morphology of a metal film after the second polymerization of PMMA was investigated in this work. The thin metal film appeared fractured after the treatment, showing an interesting complexity due to the presence of two fracture system. The form and the area of the different islands were analysed with respect to the thickness of the metallic film. The physical properties describing the observed morphology were quantified and discussed.

Cu was chosen for depositions because of its cheap cost and practical facility of evaporation, while PMMA for a good sticking coefficient. The studied samples were squared of 250 mm of side and 8 mm of complete thickness, being of suitable dimension in the production of small objects.

2. EXPERIMENTAL

Substrates of PMMA were supplied by Fratelli Guzzini s.p.a. (http://www.fratelliguzzini.com/), Recanati, Italy, to obtain new composite materials for illumination systems. Substrates started as big plates of (1500×2000) mm^2 and 3 mm of thickness. Then each plate has been cut in many squares of (250×250) mm^2. This dimension resulted to be very similar to that of many Guzzini's houses articles and, in addition, very suitable for the vacuum chamber and the crucible geometry.

The vacuum chamber was constituted by a bell of 350 mm of diameter and 500 mm of height, the vacuum system was constituted by a rotative pump coupled to a turbo-molecular. The final vacuum of 10^{-6} Torr was easily obtained. The deposition system was composed by a Mo

*Corresponding author. Tel.: +39-07535132; fax.: +39-0734656194.
E-mail address: *c.fidani@virgilio.it* (C. Fidani)

crucible BD 482009-T filled to obtain an emission area of (10×5) mm^2. PMMA temperature of samples was increased by the crucible irradiation during the metal deposition. The evaluation of the thickness was made through the sensor crystal INFICON 008-010, which position is shown in Fig. 1 with the geometry of the experimental deposition system.

Starting from the measurement of the thickness S_0 detected on the sensor position, the thickness of any other point on the plate surfaces can be calculated [8]. Introducing an (x, y) system of coordinates, as shown in Fig. 2, the $x = 0$ is put on the centre of the plate surfaces. If L_0 is the distance between the crucible and sensor and $L(y)$ the distance between the crucible and the axes of the plate with $x = 0$, one can calculate the metal thickness in any point. If AE and AD are the section areas of emission and deposition perpendicular to the atomic beam, the effective areas of emission is indicated by $AE_{eff}(x, y)$ perpendicular to the beam and that of deposition by $AD_{eff}(x, y)$. These areas can be related to the slope of the beam with respect to the plate and crucible planes. Then it is:

$$S(x,y) = S_0 \times \frac{L_0^2}{x^2 + L^2(y)} \times \frac{A_{e}(x,y)}{A_{e}(x,y)} \times \frac{A}{A} \qquad (1)$$

and it can be calculated approximately as:

$$S(x,y) \approx S_0 \times \frac{(d + c\cos\alpha)L^2(y) - d^2(1+d)}{2c^3(y)} \times \left[\frac{(x+c)L_0^2}{\sqrt{(x+c)^2 + L^2(y)}} + \frac{(x-c)L_0^2}{\sqrt{(x-c)^2 + L^2(y)}} \right], \qquad (2)$$

where $L(y) = [y^2 + a^2 + b^2 + 2ay - 2b(a + y)\cos\alpha]^{1/2}$, and $d = b - (a + y)\cos\alpha$. In the presented configuration, $2c = 10$ mm was the length of the crucible, $a = 24.4$ mm and $b = 153.9$ mm were distances defined from the geometry of the deposition system, finally $\alpha = 55°$ was the inclination of the plate. The contour graphics of (2) with the above mentioned constants is shown in Fig. 2, where the grey colour is progressively clearer for thickness more and more thicker. With a Cu thickness of 30 nm measured on the sensor, one can calculate 10 nm – 70 nm of Cu films thickness on the plate, distributed as shown in Fig. 2.

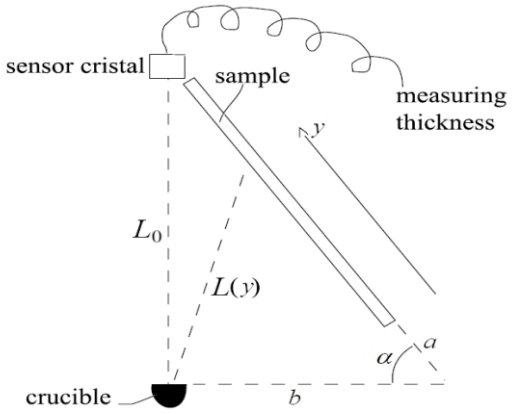

Fig. 1. Schematic experimental system located inside the vacuum bell, the section is shown for $x = 0$

The polymerization after metallisation was realised in the Guzzini's electrical oven. The pre-polymer was prepared by mixing the monomer, of chemical formula $–CH_2–C(CH_3)(COOCH_3)–$ [9], with the catalyst azoisobutyrronitrile (AZDNM). The plates with the films were fixed between two crystal surfaces separated by a space of 2.5 mm. Then, the pre-polymer was poured to fill the empty spaces between crystal-polymer and crystal-film surfaces to build a $(2.5 + 3 + 2.5)$ mm sandwiched structures. The polymerization was obtained by maintaining a constant and uniformly distributed temperature of 60 °C for four hours, then the temperature was increased up to 105 °C for one hour to check the complete polymerization of the monomer.

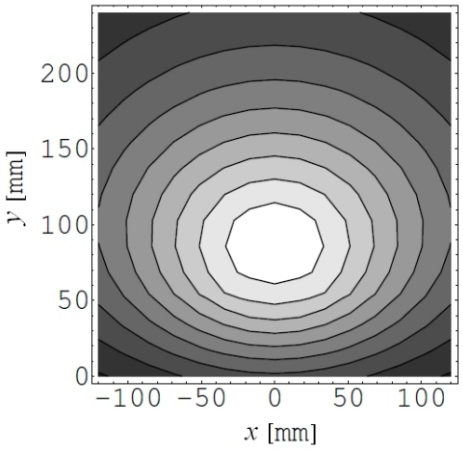

Fig. 2. The contour graphics of the deposited thickness $S(x, y)$ computed according (2). It reflects the observed symmetry of the metal deposition

To study the fractured surfaces several photos were realized in transmission light, using the microscope OLYMPUS BX60 together with a photo camera OLYMPUS DP10. The format of the areas photos was 20 mm × 15 mm, with an image definition of 640 pixels × × 480 pixels corresponding to 32 pixels/mm. This size has been chosen to cover the smallest area containing the maximum number of structures with a near constant thickness. Special attention has been devoted on focusing camera images, because depth-of-field must cover the whole depth of secondary fracture system. Larger field photos were made with a normal photo camera with zoom objectives, then the photos were converted to digital images by a scanner. The photos were manipulated and analysed by two programs of free software: SCIONIMAGE (http://scion-corporation.software.informer.com/routine) to study the areas of fracturing and FDC2D (http://wuarchive.wustl.edu/ /packages/architec/Fractals/FDC2D.sea.hqx) to study the fractal dimension. All of images were manipulated to obtain grey scale colours with better contrast.

3. MORPHOLOGY OBSERVATIONS

Cu thermally evaporated at room temperature on PMMA plates evolves progressively from small droplets up to the formation of a continuous thin film [10 – 12]. Then, the surfaces appeared completely mirror in the centre of the sample while showing a partial reflection on the corners, where it was observed a marked transparency due to the reduced thickness of the film.

After the second polymerization was concluded, the Cu films resulted completely fractured. Although, the

fractures were not uniformly distributed on the surface and forming complex structures. Starting from the surface regions corresponding to Cu minimum thickness, on the right and left corners on the top, and moving toward the centre of symmetry of Fig. 2, an increase of the island average area was observed. However, each island has become fractured moving nearer the centre of symmetry, creating an additional complex fracturing visible in Fig. 3. The pattern of the fracture system has shown a symmetry very similar to that reported in Fig. 2. Moving from the centre toward the bottom of Fig. 2, the principal islands decreased becoming very small, while the secondary fractures disappeared.

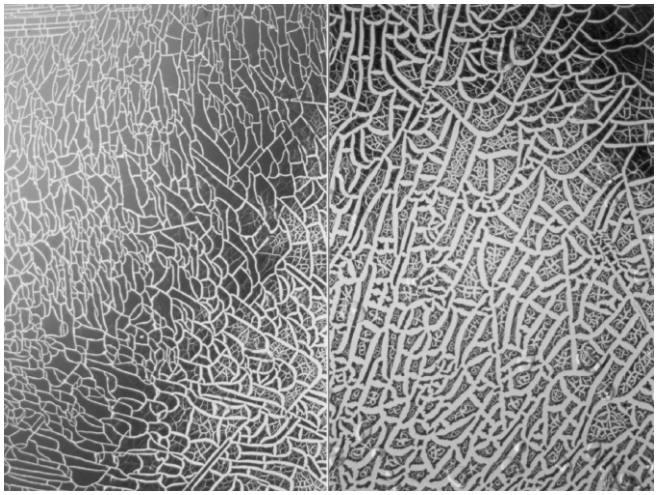

Fig. 3. Photos of two zones of the sample in transmitted light after the second polymerization. The photos reported on the left covers an area of (120×90) mm^2 while that on the right covers an area of (90×60) mm^2

The secondary fracture system appeared with different morphology having contours rounded off, whereas the primary fracture presented with very sharp broken lines. It was possible to observe an irregular film profile looking at a section of the sandwich structure at some positions. This irregularity was observed in correspondence of the secondary fracture system. Such system was characterised by Cu island edges folded towards the second polymerization, and occupied the third dimension principally around the centre of the Fig. 2. Folding was responsible of apparent rounded off contours. Irregularity thickness reached 2 mm around the centre of the Fig. 2. The width of the fractures of the principal fragmentation increased in this region because the surface area of the sample was the same while the area of the metal film occupied the third dimension.

A sharp fragmentation occurred at the bottom position of Fig. 2. This appeared difficult to explain following the Cu thickness only, because it has a different symmetry. However, the sharp fragmentation can be correlated to the modulus of the gradient of the thickness, which is shown in the contour plot of Fig. 4, a. The fracturing increased where there were strong changes of the thickness. The principal fractures were observed to diverge from the centre of symmetry of sample, follows the vector field of the gradient plotted in Fig. 4, b. The longer size of the islands were directed along the same direction.

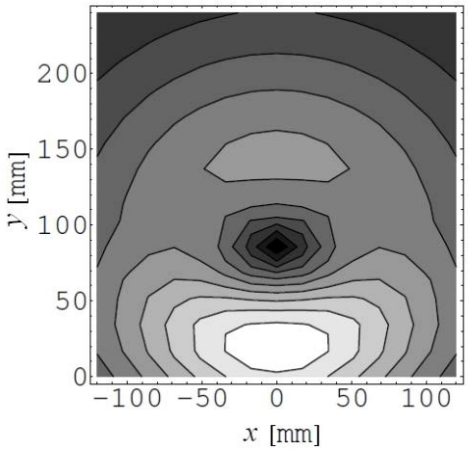

a

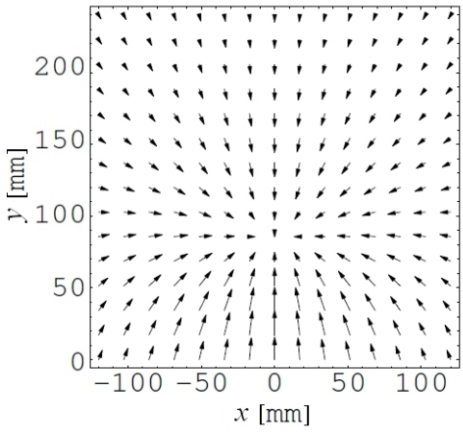

b

Fig. 4. Contour plot of the modulus of the gradient of the thickness (a) and vector field plot of the same gradient (b)

The surface of the film appeared not smooth when observed in reflection light. Film surface irregularities were observed on all the region samples, and they were very fine on the corners on the top of Fig. 2, while they were coarser where size of the area of the islands had got a maximum. The secondary fracture system prevented to observe the irregularities of the Cu islands near the centre of the sample. To obtain a more quantitative law on the fragmentation, some graphical methods of analysis such as the area analysis and the fractal analysis were used.

4. ANALYSIS AND DISCUSSION

A digital analysis of the fractured Cu film was conducted. The file images created by the photo camera were initially converted in grey scale, then increased the contrast and converted in binary files. The results are shown in Fig. 5, a, and Fig. 6, a. After this procedure, the island's area sizes were analysed employing SCIONIMAGE routine. It was set choosing the minima considerable size. This procedure was very important to eliminate the imperfections of image. In addition, particles touching edge images were ignored while interior island holes were included. The analysis gave the characteristic wideness of the islands in the different regions by distribution, average and standard deviation. Distributions $n(A)$ with respect to the number of the islands of area A,

relative to the areas reported in Fig. 5, a, and Fig. 6, a, are shown respectively in Fig. 5, b, and Fig. 6, b. They are Poissonian distributions.

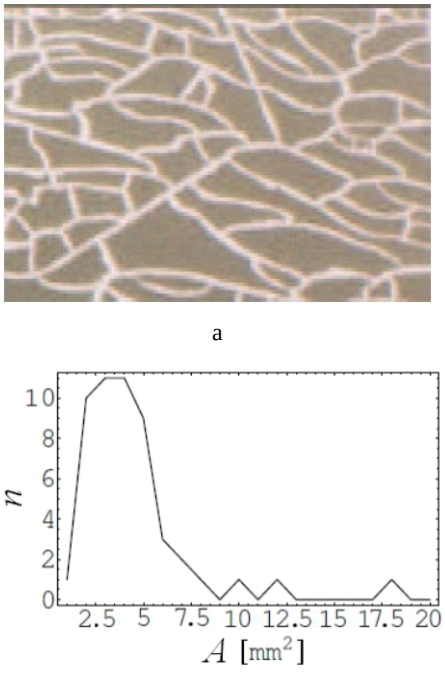

a

b

Fig. 5. A photo, in transmitted light, of a zone of the sample where the thickness was 22 nm (a) and the distribution of the areas of the islands with mean value of 3.4 mm^2 (b)

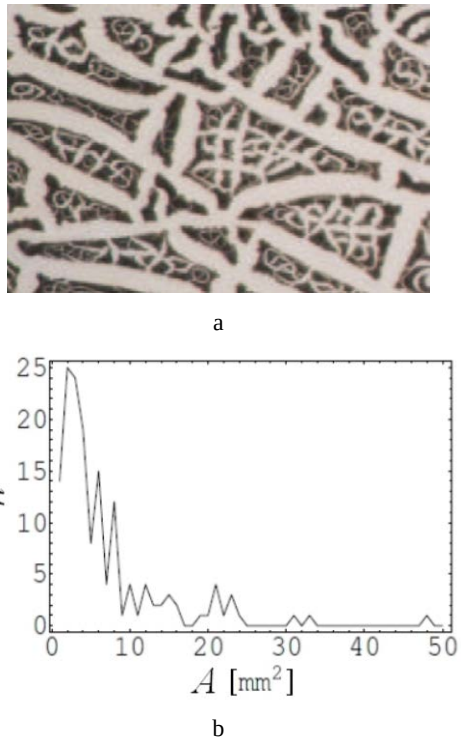

a

b

Fig. 6. A photo, in transmitted light, of a zone of the sample where the thickness was 64 nm (a) and the distribution of the areas of the islands with mean value of 0.6 mm^2 (b)

The plot of the area average values as a function of the thickness of the film is reported in Fig. 7. This shows a monotone increasing area of the islands up to the centre of the sample, where Cu thickness was maximum. These islands are delimited by the principal fracture system. The maximum island area was about 7.6 mm^2 and it occurred for Cu thickness greater than 50 nm. Looking to Fig. 3, islands appear to be divide by a secondary fracture system where Cu thickness overcame 42 nm. Therefore, the true maximum area of islands is observed at 42 nm thickness. These true maximum area islands follows the profile with the same thickness of Fig. 2, as it is confirmed by Fig. 3. The standard deviation has also a maximum for Cu thickness corresponding to 42 nm. Finally, a monotone decreasing of the island areas created by secondary fracture system is shown in Fig. 7 right down, it starts with island areas of about 1 mm^2.

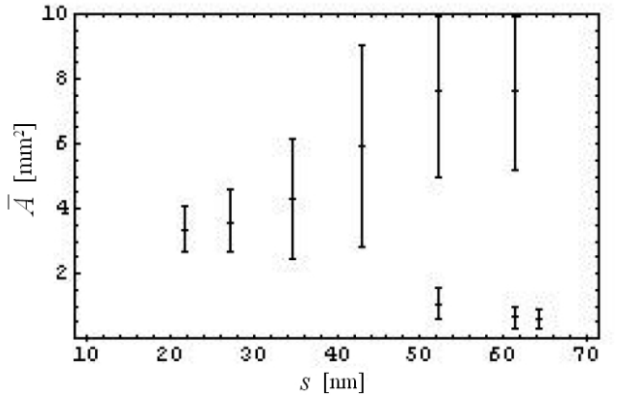

Fig. 7. Mean area and standard deviation with respect to the thickness calculated from the analysis of many sample photos

Interestingly, if the primary fracture system is compared with the modulus of the Cu thickness gradient shown in Fig. 4, a, it is possible to observe areas to become smaller where the plot is white. In other terms, the areas size of the islands also depends from the Cu thickness variation. The effect starts to be effective in the white area of Fig. 4, a, which is equivalent to overcome 5 nm/mm as shown in Fig. 8. Decreasing area is responsible for standard deviation maximum as white region is crossed by 42 nm Cu thickness.

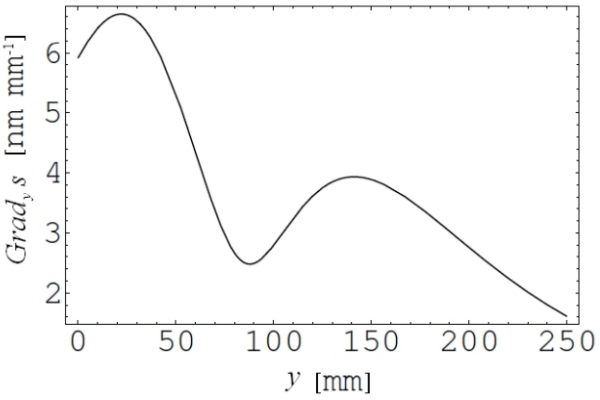

Fig. 8. Plot of the absolute value of the thickness gradient along the direction x = 30 mm where all the photos were taken

A further digital treatment was necessary to analyse the fracture system. Because the fractures are of finite thickness, we have to modify the images to obtain a skeletrisation. The images were converted in a grey scale, enhanced in contrast, converted to binary file to obtain the negative photo and then skeletrised with SCIONIMAGE options. The results of

these procedures are shown in Fig. 9. PAINT SHOP PRO resulted to be very useful to delete many imperfections introduced by the conversion and it was suitable to convert the format file of image in PICT for Mac. FDC2D performed the log[1/*s*] and log[*n*(*s*)] analysis, being *s* the dimension of the box counting and *n*(*s*) the number of the boxes necessary to cover all the graphics.

The analysis revealed the fracture system geometry of the metal film to be a fractal. An example of the scale invariance of film fractures was reported in Fig. 10, where the fractal dimension is defined as the angular coefficient of the straight line that fits the values of the analysis of Fig. 9, b. Dimension was scale invariant between 2 mm and 20 mm for the principal fracture system while it extended between 0.8 mm and 20 mm for the whole fracture primary plus secondary systems. The fractal dimension was calculated between 1.55 and 1.63 for the principal fracture system, while it was calculated between 1.55 and 1.7 for the whole structure, comprising the secondary system as well. Interestingly a minimum in the fractal dimension was observed in close correspondence to the transition between the two systems.

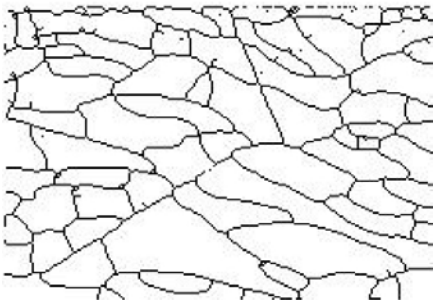

a

b

Fig. 9. Graphical preparation to the fractal analysis: a – was relative to the photo of Fig. 5, a; b – was relative to the photo of Fig. 6, a

The different thermal dilatation coefficients of the two materials must be considered to explain the origin of film fractures. In fact, the second polymerization was obtained by increasing the temperature of the sample up to 60 °C. Dilatation coefficient of Cu films is 17.7 ppm/ °C [13], equal to the bulk Cu dilatation coefficient, while for bulk PMMA the dilatation coefficient is 90 ppm/ °C [14]. Being so, Cu film experienced fractures because of the strain field applied by PMMA major expansion. The primary fracture system having increasing size of the island areas with the film thickness occurred because the increasing cohesion of Cu [15].

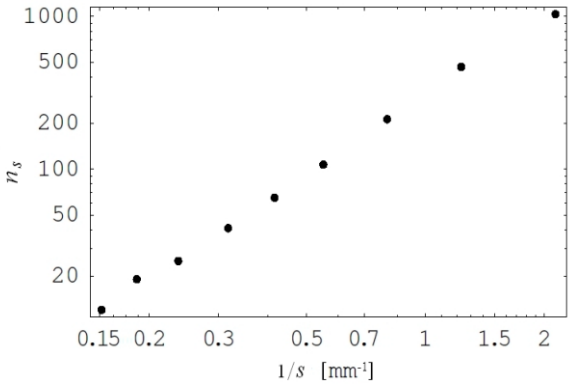

Fig. 10. The measurements of the fractal dimension of the fracture system of the photo in Fig. 6, a, was made by box counting of Fig. 9, b, the geometry shown to be scale invariant between 0.8 mm and 20 mm

To understand the secondary fracture system, it can be considered that metal adhesion on PMMA improves with increasing temperature [16]. Chemical reactions at the metal/polymer interface were usually discussed in terms of carbon-oxygen bond-breaking of the carboxylic group giving rise to C–O–Metal groups [17] or the formation of a charge transfer complex, as has been claimed in metallised polyimide samples [18]. However, the chemical bonding was considered weak in Cu/PET samples and adhesion strength correlated with the metal diffusion into the polymer layer to form clusters [16, 19]. PMMA was heated by the crucible high temperature due to the proximity of the sample for irradiation. Starting at room temperature, in the range between 80 °C – 120 °C, it was observed that the metal adhesion increased very rapidly from 240 g in^{-1} up to the upper limit value of 1300 g in^{-1} [16]. So, the in-plane film traction was created during the sample polymerization in the oven, and it was greater in the region with major adhesion. Increased adhesion thus produced the secondary fracture system.

Then, the action of chemical melting from the monomer on the polymer can be consider. Because the specific weight of the monomer is 0.92 while that of the polymer is 1.2 [14] an increase of substrate volume should be expected where the contact area between the pre-polymer and PMMA occurred, in the fracture spaces. The substrate volume increasing folded the Copper island edges towards the pre-polymer, with a consequent increasing size of the fractures.

Scale invariance of two fracture systems can indicate that the same process is fracturing at different dimensions, which is the stress due to different dilatation coefficients. The minimum fractal dimension near to 42 nm of Cu thickness can be interpreted as due to the opposite contribute to island fragmentation of the increasing metal thickness and the increasing adhesion to PMMA.

5. CONCLUSIONS

Thin film fracturing morphologies of Cu in polymer composite sandwich structures were digitally investigated. The thin film morphology, after the polymerization, consisted of two fracture systems giving rise to two different island's area sizes. Surface stress effects during the polymerization were considered to yield the fractures,

because of different thermal expansion coefficients of Cu and PMMA, depending from Cu thickness and adhesion to the polymer surface. A folding of Cu film island edges was explained with the monomer action on the PMMA in the fracture areas. Cu thickness was simulated with a mathematical model and compared with the fracture pattern. Island areas and fractal dimension of the fracture systems were quantified by digital analysis, so to know the parameter to reproduce the same aesthetic effect.

The sandwiched structures were prepared with the objective to create new diffused light effects as lampshades produced by the Company *iGuzzini* for Indoor lighting and outdoor lighting luminaries (http://www.iguzzini.com/).

Acknowledgments

The financial assistance given by Guzzini s.p.a. is gratefully acknowledged. Acknowledgement to R. Bernardini for the several suggestions to the deposition of the films, G. Pisauri for the achievement of the polymerization and the XAS group of the Camerino University for the apparatus and the assistance.

REFERENCES

1. **Wooten, F.** Optical Properties of Solids, Springer, Academic Press, 1972.
2. **Mittal, K. L.** (Ed.) Metallized Plastics 1 – 5; Fundamental and Applied Aspects, Plenum New York, 1991-7.
3. **Taga, Y.** Recent Progress of Nanotechnologies of Thin Films for Industrial Applications *Materials Sciences and Engineering C* 15 2001: pp. 231 – 235.
4. **Goswami, S., Becker, W.** Analysis of Debonding Fracture in a Sandwich Plate with Hexagonal Core *Composite Structures* 49 (4) 2000: pp. 385 – 392.
5. ENGELHARD CORPORATION in**:** Industrial Grade Pearlescent Pigments Color Card Catalougue, Pigments & Additives Group, Iseline, New Jersey, 1997.
6. **Fendler, J. H., Tian, Y.** Nanoparticles and Nanostructured Films. J. H. Fendler (ed.), WILEY-VCH, 1998. http://dx.doi.org/10.1002/9783527612079
7. **Mattox, D. M.** Handbook of Physical Vapor Deposition (PVD) Processing. 2nd edition, Elsevier, 2010.
8. **Sacher, E., Kowalczyk, S. P., Pireaux, J.-J.,** Metallization of Polymers. Oxford University Press, 1990. http://dx.doi.org/10.1021/bk-1990-0440
9. **ATO,** elf autochem NORSOCRILMMA. July, 1993.
10. **Lewis, B., Anderson, J. C.** Nucleation and Growth of Thin Films. Academic, New York, 1978.
11. **Yu, X., Duxbury, P. M., Jeffers, G., Dubson, M. A.** Coalescence and Percolation in Thin Metal Films *Physical Review B* 44 1991: pp. 13163 – 13166.
12. **Adams, J. B., Wang, Z., Li, Y.** Predicting the Microstructure of Cu Thin Films *Thin Solid Films* 365 2000: pp. 201 – 210. http://dx.doi.org/10.1016/S0040-6090(99)01047-0
13. **Zhao, J.-H., Du, Y., Morge, M., Ho, P. S.** Simultaneous Measurement of Young's Modulus, Poisson Ratio, and Coefficient of Thermal Expansion of Thin Films on Substrates *Applied Physics* 87 2000: pp. 1575 – 1577.
14. **Lide, D. R.** Handbook of Chemistry and Physics. 72nd Edition, CRC Press, 1991–1992.
15. **Streitz, F. H., Cammarata, R. C., Sieradzki, K.** Surface-Stress Effects on Elastic Properties. I. Thin Metal Films *Physical Review B* 49 1994: pp. 10699 – 10706.
16. **Silvain, J. F., Ehrhardt, J. J.** An Overview on Metal/PET Adhesion *Thin Solid Films* 236 1993: pp. 230 – 235. http://dx.doi.org/10.1016/0040-6090(93)90675-F
17. **Atanasoska, Lj., Anderson, S. G., Meyer III, H. M., Lin, Z., Weaver, J. H.** Aluminum/Polyimide Interface Formation: An XPS Study of Selective Chemical Bonding *Journal of Vacuum Science and Technology A* 5 (6) 1987: pp. 3325 – 3333. http://dx.doi.org/10.1116/1.574191
18. **Haight, R., White, R. C., Silverman, B. D., Ho, P. S.** Complex Formation and Growth at the Cr- and Cu-Polyimide Interface *Journal of Vacuum Science and Technology A* 6 (4) 1988: pp. 2188 – 2200. http://dx.doi.org/10.1116/1.575010
19. **LeGoues, F. K., Silverman, B. D., Ho, P. S.** The Microstructure of Metal-Polyimide Interfaces *Journal of Vacuum Science and Technology A* 6 (4) 1988: pp. 2200 – 2205. http://dx.doi.org/10.1116/1.575011